Available online at www.sciencedirect.com
SCIENCE DIRECT
Journal of Photochemistry and Photobiology A: Chemistry 172 (2005) 19–26
Journal of Photochemistry and Photobiology A:Chemistry
www.elsevier.com/locate/jphotochem

Photocatalytic activity of sol–gel derived titania converted into nanocrystalline powders by supercritical drying

Yu.V. Kolen'ko[a,c], A.V. Garshev[a], B.R. Churagulov[b], S. Boujday[c], P. Portes[c], C. Colbeau-Justin[c,*]

[a] *Department of Materials Science, Moscow State University, Moscow 119992, Russia*
[b] *Department of Chemistry, Moscow State University, Moscow 119992, Russia*
[c] *Laboratoire d'Ingénierie des Matériaux et des Hautes Pressions (CNRS, UPR1311), Université Paris 13, 99 Av. J-B Clément, Villetaneuse 93430, France*

Received 29 July 2004; received in revised form 3 November 2004; accepted 4 November 2004
Available online 9 January 2005

Abstract

Nanocrystalline (14–18 nm) anatase TiO_2 powders with high photocatalytic activity are synthesized by a sol–gel method followed by supercritical drying in isopropanol. The photocatalytic behavior is studied in the model reaction of phenol photodegradation in water. The relationship between photoactivity, crystal structure, texture, charge-carrier lifetimes, bandgap energies and thermal treatment of products is discussed. The effective method of synthesis of photocatalysts based on TiO_2—sol–gel method followed by supercritical drying in isopropanol is presented. It shows, that the obtained powders can be used in photocatalytical depollution without additional thermal treatment.

Keywords: TiO_2 photocatalysis; Phenol photodegradation; Sol–gel; Supercritical drying; Charge-carrier lifetimes; Bandgap energies

1. Introduction

Titanium dioxide exists in three major modifications: rutile (tetragonal), anatase (tetragonal), and brookite (orthorhombic) [1]. Rutile is the most stable phase, however, anatase and brookite are commonly formed in metastable fine grained (nanocrystalline) synthetic and natural samples. Anatase and brookite transform to rutile upon heating.

The rutile phase is widely used as a white pigment because of its excellent scattering abilities. TiO_2 can be used for beam splitters, optical coatings and antireflection coatings because of its high dielectric constant and refractive index [2]. Titania is also used as semiconductor [3], as catalyst [4] and for solar-energy conversion [5]. Electrical characteristics of titania depend on oxygen partial pressure, therefore, it can be used as a gas sensor [6,7].

Photoelectrochemical decomposition of H_2O over TiO_2 into H_2 and O_2 [8] initiated a great wave of research activity, continuing till the present time. Anatase and rutile have been used in photocatalytic investigations dealing with photodegradation of organic pollutants in water and air [9–15]. Both phases are semiconductors with a bandgap of 3.23 eV for anatase and 3.10 eV for rutile [16]. Under UV irradiation, absorption of a photon with higher energy than the bandgap creates an electron and hole. If the charge-carriers do not recombine, they can migrate on the surface where the electrons are trapped by titanium while the holes are trapped by the hydroxyl surface groups. Then, the trapped holes form radicals $OH^\bullet$ and the trapped electrons react with O_2 and H_2O forming $HO_2^\bullet$ radicals. These free radicals cause the oxidation of organic compounds, such as phenol [10].

There is no general agreement on the criteria that have to be used for a correct comparison of the different photocatalytic system performances. Surface and bulk

* Corresponding author. Tel.: +33 1 49 40 44 88; fax: +33 1 49 40 34 14.
E-mail address: colbeau@limhp.univ-paris13.fr (C. Colbeau-Justin).

1010-6030/$ – see front matter © 2004 Elsevier B.V. All rights reserved.
doi:10.1016/j.jphotochem.2004.11.004

properties and photoactivity depend strongly on a method used for the preparation of materials. A direct correlation between photoactivity and surface properties is not possible, and it has been shown that the photoactivity of titania is influenced by the phase composition, crystalline quality, morphology, particle size, size distribution, high surface area, porosity, surface hydroxyl density and bandgap [9–15].

We have chosen a sol–gel method followed by supercritical drying in isopropanol to synthesize TiO_2 photocatalysts. The motivation to combine a sol–gel technique with a supercritical drying was to control the preparation of solids with interesting textural, chemical and morphological properties [17–20]. The advantages of the sol–gel technique are molecular-scale mixing of the components, high purity of the precursor, and homogeneity of sol–gel products with high isotropy of physical, morphological and chemical properties. For supercritical drying, two basic ways are nowadays applied—high-temperature techniques and various low-temperature methods [21].

In a previous work, we reported the synthesis of TiO_2 by sol–gel method followed by supercritical drying in carbon dioxide [22]. With this treatment, the obtained powders are amorphous, and a thermal treatment is necessary to crystallize. In the case of isopropanol, the drying is realized at 350 °C and a crystallized powder is expected. It is important that powders received by high-temperature technique could be used as catalysts directly after drying without an additional thermal treatment.

Here we report the photocatalytic properties of nanocrystalline titania powders prepared by sol–gel method followed by supercritical drying in isopropanol. We compared our samples to those obtained after supercritical drying in carbon dioxide, and to the commercial compound P25 from Degussa. The relationship between photoactivity, structure, texture, charge-carrier lifetimes, bandgap energies, and thermal treatment of the products is discussed.

2. Experimental

2.1. Titania preparation

Sol–gel preparation of titania gel was based on the route elaborated by Dagan and Tomkiewicz [23]. Firstly, alkoxides precursor (tetraisopropoxytitanium (IV) $Ti(O–iC_3H_7)_4$, Acros, 98%, 18.58 ml) was dissolved in absolute ethanol (Prolabo, 99.85%, 51.00 ml). The hydrolysant consisted of distilled water (0.87 ml) and 2 M aqueous nitric acid solution (Prolabo, 69%, 2.5 ml) diluted in absolute ethanol (15 ml). The hydrolysant was added drop-by-drop to the alkoxides solution at room temperature under continuous stirring (400 rpm). The molar ratio alkoxide/alcohol/water/acid was 1/18/3/0.08. Within 30 min, monolithic, transparent TiO_2 alcogel was obtained. The resulting gel was aged for 12 h at room temperature.

To obtain the powder from alcogel, we performed drying under supercritical conditions of iC_3H_7OH (T_c = 235.1 °C, P_c = 47.6 bar, ρ_c = 0.273 g/cm^3). When the pore liquid is removed as a gas phase from the interconnected sol–gel network under supercritical conditions (critical-point drying method), the network does not collapse and a low density aerogel is produced. Alcogel was put into a stainless steel autoclave (volume, 150 ml; degree of filling by iC_3H_7OH, 80%). The solvents present in the alcogel (EtOH, H_2O and iC_3H_7OH) were replaced by iC_3H_7OH flow of 5 ml/min for 1 h at a pressure of 100 bar and a temperature of 300 °C. At the end of supercritical drying, the autoclave was removed from the furnace and cooled down to room temperature.

Drying under supercritical conditions of CO_2 (T_c = 31 °C, P_c = 73.8 bar) have been performed previously [22]. Alcogel was put in the same autoclave as drying in isopropanol. The alcohol contained in the gel was replaced with liquid CO_2 and then, the system was brought above the critical point for 15 min, at a pressure of 70 bar and a temperature of 50 °C. At the end of supercritical drying, the autoclave was removed from the furnace and cooled down to room temperature.

After supercritical drying, off-white TiO_2 (∼5 g) was obtained. To remove most of the organic residues, a thermal treatment of the sample was carried out at 450, 500, and 550 °C in air. The treatment included a 6 h heating up to the final temperature and a 10 h ramp.

Throughout this work, a set of acronyms is used: NI, NI450, NI500, NI550 and NA550. The N refers to the nitric acid used to form the gel, I the supercritical drying in isopropanol, and A to the supercritical drying in carbon dioxide. The heating temperature is indicated at the end of each reference.

2.2. Characterization and property measurements

Powder X-ray diffraction (XRD) was carried out using Cu Kα radiation (DRON-3M diffractometer). The size of TiO_2 crystallites was estimated by means of the Scherrer's equation from broadening of the (1 0 1) anatase reflection. IR spectra were collected with a FTIR Perkin-Elmer Spectrum One spectrometer. Diffuse reflection (DR) spectra were recorded on a Perkin-Elmer Lambda 35 UV–Visible Spectrophotometer using a diffuse reflection cell. Powders morphology were analyzed using scanning electron microscopy (SEM; LEO 440S, Leica, Cambridge) and transmission electron microscopy (TEM; JEOL JEM FX2000II). The specific surface area and pore size distribution were measured by the BET and BJH methods using nitrogen physisorption at 77 K (COULTER SA 3100). Thermogravimetric analysis (TGA) was performed using PYRIS Diamond TG-DTA thermoanalyser (Perkin-Elmer), in air, with a heating rate of 10 °C/min. The carbon content was determined by conventional elemental analysis.

2.3. Electronic properties characterization

Lifetime of charge-carriers created by UV irradiation in TiO_2 has been determined by microwave absorption using time resolved microwave conductivity (TRMC) [24–26]. This method is based on the measurement of microwave backscattering.

The experimental TRMC set-up was described in a previous work [24]. Incident microwaves were generated by a Gunn diode (K_a band, 28–38 GHz). The experiments were performed at 31.4 GHz. The pulsed light source was a Nd:YAG laser providing an IR radiation ($\lambda = 1064$ nm). Full width at half-maximum of one pulse is 10 ns, frequency of the pulses is 10 Hz. UV light (355 nm) is obtained by tripling the IR radiation. The light energy density received by the sample is 1.3 mJ cm^{-2}.

A TRMC signal can be characterized by two parameters: a maximum intensity value (I_{max}) and its decay intensity $I(t)$. I_{max} reflects the number of the excess charge-carriers created by the UV pulse. It must be noted that this information is weighted by the mobility of the charge-carriers and by the fast decay processes during the excitation (i.e. the first 10 ns), and these contributions cannot be separated easily for a system like TiO_2 powders. Since the signal decay is not purely exponential, the general decay shape is characterized by several halftime lives, $\tau_{1/2}$ is the time to obtain an intensity $I_{max}/2$ of the signal, $2\tau_{1/2}$ to obtain $I_{max}/4$ and $3\tau_{1/2}$ to obtain $I_{max}/8$. As recombination phenomena occur mainly between 0 and 40 ns after the pulse [24], the ratio of the intensity of the signal (40 ns) after the pulse beginning by I_{max} notifies a speed of recombination processes. A high $I_{40\,ns}/I_{max}$ ratio indicates a low speed recombination. In general, a high value of I_{max} and long decay can be considered to reflect a well-crystallized structure of the sample which may involve appropriate photocatalytic properties.

2.4. Photocatalytic tests

In order to test photocatalytic behavior of the synthesized TiO_2 powders, photodegradation of phenol in water has been chosen as a test reaction as described in our previous paper [27]. An amount of 400 mg of TiO_2 powder was added in the initial 400 ml phenol (Aldrich 99%) aqueous solution ($C = 50$ mg/l, pH = 6), Vigorous stirring (900 rpm) and oxygen bubbling (20 ml/min) was started prior to the mixture exposition by an ultraviolet mercury lamp (Cathodeon HPK 125 W). The samples were withdrawn after various reaction times (0, 10, −60, 75 and 90 min). After filtration through a 0.20 μm pore size membrane PTFE filter (TITAN), the absorption spectra of phenol solution were recorded between 200 and 600 nm. For measuring phenol concentration, the CARY 300 Scan UV–visible spectrophotometer was used at $\lambda = 269$ nm corresponding to the maximal adsorption of phenol. Concentrations of phenol in water were calculated using the Lambert–Beer law [28].

3. Results and discussion

Thermal treatment, drying conditions, phase composition, particle size, specific surface area, pore volume, and bandgap energy of nanocrystalline titania powders prepared by sol–gel method followed by supercritical drying in isopropanol or carbon dioxide and P25 are given in Table 1.

Electronic properties, given by the values of TRMC experiments, I_{max}, $I_{40\,ns}/I_{max}$, $\tau_{1/2}$, $2\tau_{1/2}$ and $3\tau_{1/2}$, are given in Table 2.

Fig. 1 illustrates the percent of photodegraded phenol versus irradiation time of TiO_2 samples. The percentage of photodegraded phenol on titania powders after 75 min illumination time is displayed in Table 1.

3.1. Supercritical drying in isopropanol

Supercritical drying of TiO_2 alcogel in isopropanol leads to the formation of nanocrystalline anatase with particle size of 14 nm (XRD), which does not transform into rutile under a thermal treatment ranging from 450 to 550 °C for 10 h (Table 1). Line-broadening analyses for all the materials reveal that the crystallite sizes of titania powders (NI, NI450, NI500 and NI550) increase slighly from 14 to 18 nm with an increase of calcination temperature (Table 1).

The obtained powders have off-white color caused by incompletely decomposed organic products. After calcina-

Table 1
The phase composition and textural properties of titania synthesized by sol–gel method followed by supercritical drying and P25

Reference	Drying	ThT[a] (°C)	Phase composition	Particles size (nm, ±10%)		Weight loss (30–1100 °C, wt.%)	BET (m^2/g, ±5%)	BJH (ml/g, ±5%)	E_{bg} (eV, ±0.01)	Conversion of phenol[b]
			XRD	XRD	TEM					
NI	iC_3H_7OH	–	Anatase 100%	14	20	3.98	92	0.46	2.95	94
NI450	iC_3H_7OH	450	Anatase 100%	16	26	3.18	79	0.42	3.00	99
NI500	iC_3H_7OH	500	Anatase 100%	17	21	2.96	77	0.38	2.99	97
NI550	iC_3H_7OH	550	Anatase 100%	18	23	2.95	68	0.46	2.99	94
NA550	CO_2	550	Anatase 100%	21	20	3.00	63	0.26	–	92
P25	–	–	Anatase 75%, Rutile 25%	–	25	–	52	0.15	–	100

[a] Thermal treatment.
[b] Percent of degraded phenol after 75 min irradiation time.

Table 2
The electronic properties (TRMC) of titania synthesized by sol–gel method followed by supercritical drying and P25

Reference	I_{max} (mV)	$I_{40\,ns}/I_{max} \times 100$ (%)	$\tau_{1/2}$ (ns)	$2\tau_{1/2}$ (ns)	$3\tau_{1/2}$ (ns)
NI	23.1	53.4	40	220	1000
NI450	33.4	41.0	28	128	680
NI500	35.4	44.8	29	155	790
NI550	34.4	41.6	28	127	940
NA550	17.8	56	60	3000	$>10^4$
P25	7.9	42	35	160	1500

tions at 450, 500 or 550 °C for 10 h, the samples become white. Decomposition of organic products was proved by TGA (Table 1) and elemental analysis. The maximum value of weight loss was record for the NI sample compared to NI450, NI500 and NI550 samples. This value is due, for the NI sample, to the removal of remaining decomposed and initial organic compounds. According to the elemental analysis, the sample NI contains 1.1% of carbon while the sample NI550 was carbon-free. The weight loss of the NI450, NI500, NI550 samples and, partly for NI sample, is related to removal of hydration water, OH surface groups and small amount of alkoxy groups which are oxidized at higher temperature than the temperature of calcinations.

This fact is well-proved by the FTIR spectroscopy data (Fig. 2). All the spectra show one broad band near 3400 cm^{-1} and another one near 1630 cm^{-1} which correspond to surface-adsorbed water and hydroxyl groups [29]. As it is shown in Fig. 2, the NI sample has more surface-adsorbed water and hydroxyl groups than annealed samples. However, sample NI has significant peaks around ~2924, ~1400 and ~1063 cm^{-1}, which practically disappear after thermal treatment. This group of peaks corresponds to remaining organic compounds, like *i*PrOH and EtOH. [30], which are almost fully oxidized after calcination (Fig. 2). The strong peak at 600 cm^{-1} corresponds to the infrared active mode of anatase. At the same time, there is a sharp peak at 2341 cm^{-1} for annealed samples (NI450, NI500, NI550) which is completely absent for the NI sample. This peak can be attributed to CO_2 [30]. It is believed that CO_2 is formed during the combustion of organic impurities in the NI sample, and partly adsorbs onto TiO_2 particles.

The synthesized anatase powder morphology observed by SEM and TEM is shown in Figs. 3 and 4, respectively. Significant differences are evidenced when comparing the microphotographs (Fig. 3a and b). The NI sample consists of large aggregates (Fig. 3a) which are transformed to more fine aggregates after calcination at 550 °C for 10 h (Fig. 3b). As shown in Fig. 3, the aggregated particles consist of many TiO_2 nanoparticles. TEM data revealed that the nanoparticles size slightly increases from 20 nm for NI sample to 26 nm for NI450 sample with the increase of the calcination temperature (Table 1, Fig. 4a and b). Electron diffraction for the TiO_2 samples (insets in Fig. 4a and b) shows distinct ring-like patterns indicating high crystallinity of the synthesized titania.

The BET specific surface area and BJH pore volume data of prepared TiO_2 are presented in Table 1. It is observed that the NI sample prepared by supercritical drying has a high specific surface area (92 m^2/g) which decreases significantly to 68 m^2/g for NI550 sample with increasing of the calcination temperature.

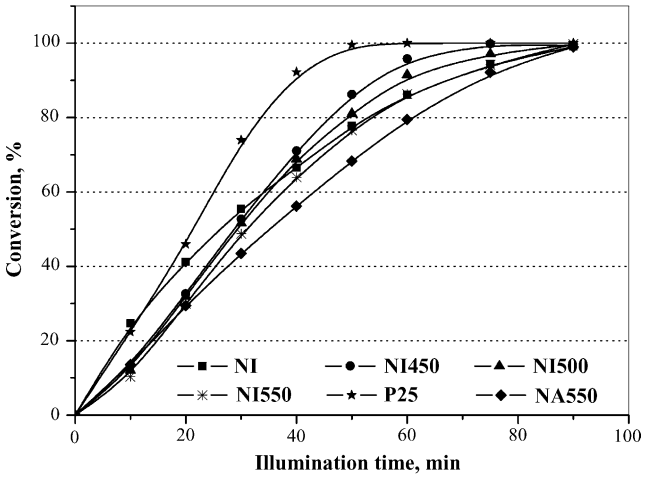

Fig. 1. Percent of degraded phenol vs. irradiation time of a TiO_2 powders prepared by sol–gel method followed by supercritical drying. Reproducibility was better than 2%.

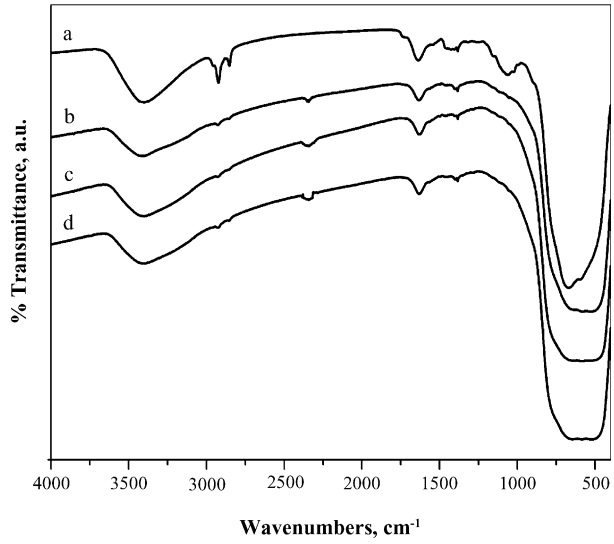

Fig. 2. FTIR spectra of titania prepared by sol–gel method followed by supercritical drying: (a) NI; (b) NI450, (c) NI500; (d) NI550.

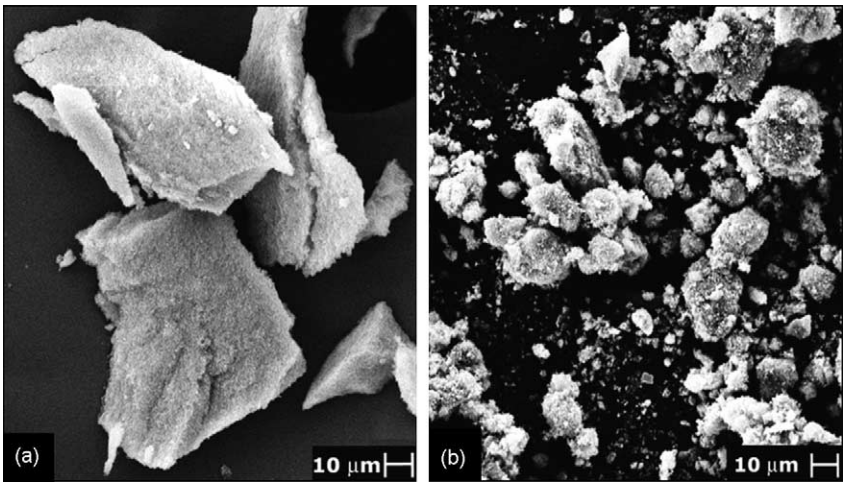

Fig. 3. SEM microphotograph of TiO_2 anatase powders prepared by sol–gel method followed by supercritical drying: (a) NI; (b) NI550.

Diffuse reflectance spectra of as-prepared powders show small differences in light absorption between the NI450, NI500 and NI550 samples. However the NI sample begins to absorb radiation at about 695 nm (Fig. 5) due to the carbonate species content (TGA, FTIR). Assuming that materials like TiO_2 are indirect semiconductors, a plot of the modified Kubelka–Munk function versus the energy of exciting light [31] gives bandgap energies of 2.95, 3.00, 2.99 and 2.99 eV for NI, NI450, NI500 and NI550, respectively (Table 1, Fig. 6). It should be noted, that diffuse reflectance spectra for NI450, NI500 and NI550 samples has a blue-shift compared to NI sample. However, usually the particles size growth results in a red-shift. This observation might be connected with organic species content [32], but also with the lattice strain in the small particles [33] for NI sample.

TRMC results (Table 2) show that the number and the lifetime of charge-carriers are almost the same for the three annealed samples. It means that the temperature of thermal treatment has no real influence on the crystalline quality. I_{max} value is slightly smaller for NI. This point must be related to the absorption spectra of NI sample: organic species absorb also the laser beam. The $\tau_{1/2}$ values indicate longer lifetime of charge-carriers and $I_{40\,ns}/I_{max}$ value indicates less recombination phenomena for NI. These points show that thermal treatment allows the degradation of organic species but is not necessary to increase the crystalline quality of the supercritically dried sample. It should be noted also that for all synthesized samples long decay time is observed.

Photocatalytic results show that the four samples dried in isopropanol induced practically complete photodegradation of phenol after 90 min (Fig. 1). The values gathered in Table 1 show that NI450 is the more active, then NI500 and follows NI550. Despite a higher initial reaction rate, the percent of phenol photodegradated after 75 min show that NI activity is quite similar to NI550.

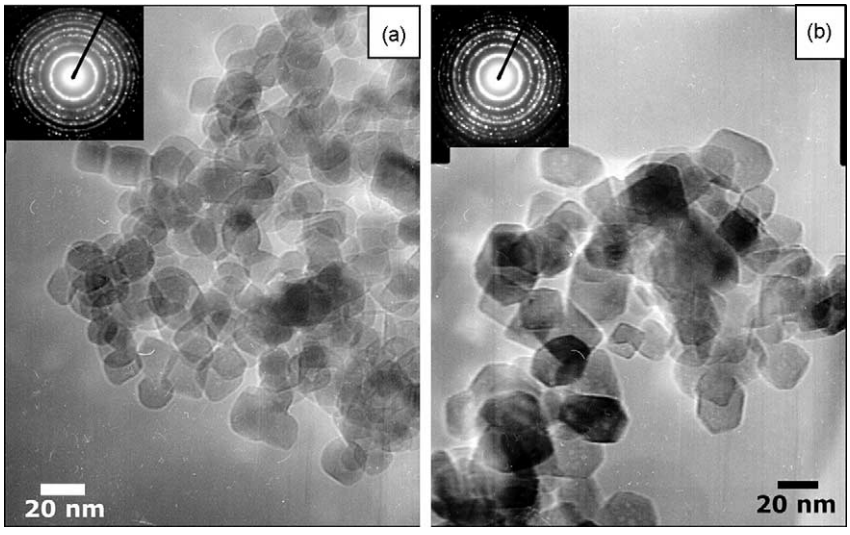

Fig. 4. TEM microphotograph of TiO_2 anatase particles synthesized by sol–gel method followed by supercritical drying: (a) NI; (b) NI550.

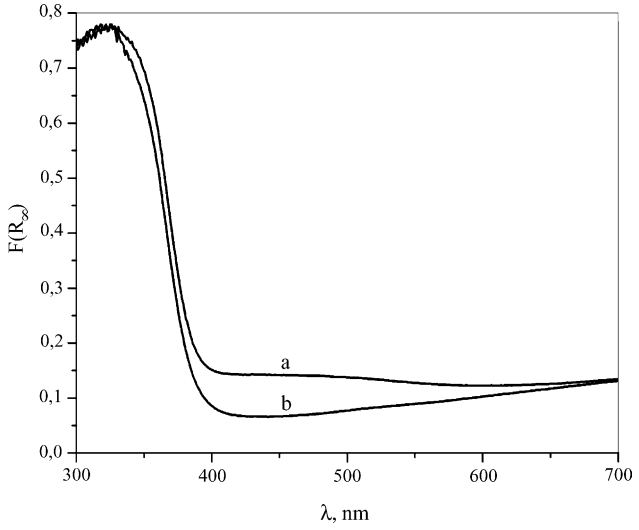

Fig. 5. Diffuse reflectance spectra of a TiO_2 powders synthesized by sol–gel method followed by supercritical drying: (a) NI; (b) NI450.

To make the correlation between the structural, textural and electronic properties of TiO_2 powders obtained by sol–gel method followed by supercritical drying and their photocatalytic activities, we can consider two linked parts of the photocatalysis mechanism [22]. The first part, the *photo part*, concerns phenomena related to the interaction of material with light. This includes photons absorption, charge-carrier creation, dynamics, and their surface trapping. The second part, the *catalysis part*, concerns phenomena of radicals formation onto the surface and 'surface reactivity', i.e. the heterogeneous interaction between H_2O, O_2, organic pollutants at the oxide surface.

For the *photo part*, the TRMC and bandgap energies measurements can be considered as an indicators of the interaction of material with light. High values of I_{max} and slow decay indicate a large amount of charge-carriers created having long lifetimes, and thus, reveal a high crystalline quality [22]. Low bandgap of titanium dioxide leads to utilization of a much larger fraction of visible light, i.e. photochemical yield is higher [29].

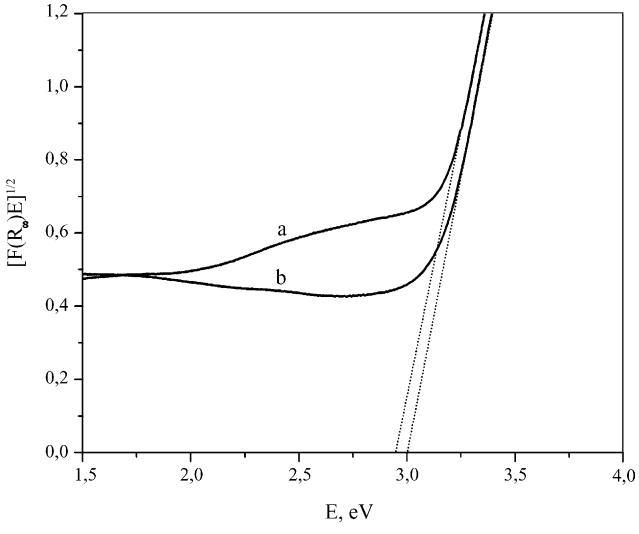

Fig. 6. Plot of transformed Kubelka–Munk function vs. the energy of the light absorbed: (a) NI; (b) NI450.

For the *catalysis part*, the specific surface area is the most effective structural parameter. Indeed, photocatalysis is an interfacial reaction. Thus, a higher specific surface area induces a higher number of accessible active sites and, consequently, better reactivity.

Concerning annealed samples, we checked before with TRMC, that the temperature of thermal treatment has no significant role on the *photo part*, it means on the crystalline quality. On the opposite, thermal treatment leads to particle size growing. NI450 sample shows the highest specific surface area, then NI500 and NI550 (Table 1). It means that increasing thermal treatment is not favorable to the *catalysis part*. As, the photocatalytic properties may be considered as resulting from the combination of these two parts, NI550 has a lower activity than NI450 because of its lower surface area.

Concerning NI sample, no post-drying thermal treatment is realized. This point is favorable to the *catalysis part* and NI shows the highest surface area. The effect on the *photo part* is less obvious. Results showed that NI is a TiO_2 phase mixed with carbonate species. Their influence on crystalline quality is not direct, but they absorb UV-light and the absorbed photons are no more available to create charge-carriers in the semiconductor for photocatalysis. The activity of NI is slightly lower than for annealed samples. Anyway, it should be emphasized that the powders synthesized by sol–gel method followed by supercritical drying in isopropanol can be used in photocatalysis without any additional thermal treatment.

3.2. Comparison with supercritical drying in carbon dioxide

In our previous work devoted to the supercritical drying in carbon dioxide, we observed an opposite behavior concerning thermal treatment. In the case of CO_2, the treatment was necessary to burn organic compounds but also to crystallize TiO_2. It means that increasing thermal treatment was necessary to promote electronic properties while it was bad for surface area. The best average was found for thermal treatment at 550 °C (NA550). In the case of supercritical drying in isopropanol, the thermal treatment is not needed to crystallize and 450 °C is enough to burn organic species, the best compound is NI450.

The comparison of the photocataytic activity of these two compounds (Table 1, Fig. 1) shows that NI450 is more active than NA550.

Structural and microstructural results gathered in Table 1 show that both phases are pure nanostructured anatase, and that the surface area and the total pore volume are higher for NI450 than for NA550. The lower temperature treatment avoids the particle growing and the collapsing of the aerogel network.

TRMC results of Table 2 show that NA550 presents a slower decay, but its I_{max} is two times lower than the NI450 I_{max} value. It indicates that the number of charge-carriers created in NA550 is less important or that most of them recombine during the pulse.

To summarize, the comparison of these two compounds shows that NI450 is more active than NA550 because of its better electronic and surface properties.

3.3. Comparison with P25

Structural, TRMC and photocatalysis results on P25 Degussa commercial powder reported in a previous work [34] are summarized in Tables 1 and 2 and Fig. 1. The results show that P25 degrades 100% of phenol after 75 min illumination. The comparison with supercritically prepared powders evidences that P25 is slightly better photocatalyst than NI450 that degrades 99% of phenol after 75 min illumination.

Therefore, P25 shows a rather low specific surface area ($52\,m^2\,g^{-1}$) and quite short time charge-carrier lifetimes. This latter result shows the limit of the simple model used with separated *photo* and *catalysis* parts. This model allows comparison between powders coming from the same kind of synthesis [22,34], and it surely helps to understand the influence of one synthesis parameter on photocatalytic properties. In the case of very different powders, other parameters like impurity level, crystallographic surface, surface defects and oxygen adsorption [35] have maybe to be taken in account.

It must be noted that P25 is a mixture of rutile and anatase. Rutile itself is a low-active phase, but the junction created by the two semiconductors helps the charge-carriers separation. It means that the carriers created in the rutile part do not rise up photoactivity like in the pure phase. The rutile phase of P25 plays only the role of charge separator and provides sites for oxidation [36,37]. In this case, P25 is difficult to compare to pure anatase phases.

4. Conclusion

In the present work, we successfully synthesized titania powders by sol–gel method followed by supercritical drying in isopropanol and investigated in details their structural, electronic and photocatalytic properties.

The relationship between the photoactivity and structure, texture, charge-carrier lifetimes, bandgap energies, thermal treatment of the products is established.

All the obtained powders are nanocrystalline anatase particles. Their activity is close to P25 if the dried sample is thermally treated at 450 °C to burn organic residues. However, it is shown that this synthesis method with high-temperature supercritical drying gives crystallized powders that can be used in photocatalysis without additional thermal treatment.

The samples have been compared to those obtained after low-temperature supercritical drying in CO_2. It is shown that in this last case, an higher additional thermal treatment is required (550 °C), to burn organic residues but also to crystallize. The comparison of these two compounds shows that the powders dried in isopropanol are more photoactive than in CO_2 because of better electronic and surface properties.

Acknowledgements

Yu.V. Kolen'ko likes to thank the INTAS Young NIS Scientist Fellowships Program 2002 (grant N YSF 2002-252) for financial support. We are also grateful to A.A. Eliseev for the FTIR spectroscopy, Dr. A.V. Olenev for fruitful discussion, and Dr. M. Kunst for his help in TRMC measurements.

References

[1] F.A. Cotton, G. Wilkinson, Advanced Inorganic Chemistry, 5th ed., Wiley, U.S.A., New York, 1988, p. 654.
[2] R.U. Flood, D. Fitzmaurisce, J. Phys. Chem. 99 (1995) 8954–8958.
[3] C.J. Chen, J.M. Wu, Mater. Sci. Eng. B 5 (1980) 377–383.
[4] S. Matsuda, A. Kato, Appl. Catal. 8 (1983) 149–165.
[5] P.V. Kamat, N.M. Dimitrijevic, Sol. Energy 44 (1990) 83–98.
[6] V. Guidi, M.C. Carrota, M. Ferroni, G. Martinelli, Sens. Actuators B 57 (1999) 197–200.
[7] G.S. Devi, T. Hyodo, Y. Shimizu, M. Egashira, Sens. Actuators B 87 (2002) 122–129.
[8] A. Fujishima, K. Honda, Nature 37 (1972) 238–241.
[9] C.S. Turchi, D.F. Ollis, J. Catal. 122 (1990) 178–192.
[10] A. Wold, Chem. Mater. 5 (1993) 280–283.
[11] E. Pelizzeti, C. Minero, Electrochim. Acta 38 (1993) 47–55.
[12] J.-M. Herrmann, C. Guillard, P. Pichat, Catal. Today 17 (1993) 7–20.
[13] D.W. Bahnemann, Res. Chem. Intermed. 26 (2000) 207–220.
[14] J. Sun, L. Gao, Q. Zhang, J. Am. Ceram. Soc. 86 (2003) 1677–1682.
[15] C.Yu. Jimmy, L. Zhang, J. Yu, New J. Chem. 26 (2002) 416–420.
[16] A.L. Linsebigler, G. Lu, J.T. Yates, Chem. Rev. 95 (1995) 735–758.
[17] A.C. Pierre, Introduction to Sol–Gel Processing, Kluwer Academic Publishers, Boston, 1998, p. 404.
[18] M. Schneider, A. Baiker, Catal. Today 35 (1997) 339–365.
[19] A.C. Pierre, G.M. Pajonk, Chem. Rev. 102 (2002) 4243–4266.
[20] K.J. Klabunde, Nanoscale Materials in Chemistry, Wiley/Interscience, New York, NY, 2001.
[21] M. Schneider, A. Baiker, Catal. Rev.–Sci. Eng. 37 (1995) 515.
[22] S. Boujday, F. Wünsch, P. Portes, J.F. Bocquet, C. Colbeau-Justin, Sol. Energy Mater. Sol. Cells 83 (2004) 421–433.
[23] G. Dagan, M. Tomkiewicz, J. Phys. Chem. 97 (1993) 12651–12655.
[24] C. Colbeau-Justin, M. Kunst, D. Huguenin, J. Mater. Sci. 38 (11) (2003) 2429–2438.
[25] M. Kunst, G. Beck, J. Appl. Phys. 60 (1986) 3558–3566.
[26] J.M. Warman, M.P. De Haas, Puls Radiolysis, CRC Press, 1991 (Chapter 6) p. 101.
[27] L. Znaidi, R. Séraphimova, J.-F. Bocquet, C. Colbeau-Justin, C. Pommier, Mater. Res. Bull. 36 (2001) 811–825.
[28] A.B.P. Lever, Inorganic Electronic Spectroscopy, 2nd repr., Elsevier, Amsterdam, 1997, p. 864.
[29] Z. Ding, G.Q. Lu, P.F. Greenfield, J. Phys. Chem. B 104 (2000) 4815–4820.
[30] K. Nakanisi, Infrakrasnie Spectry i Struktura Organicheskih Soedinenii (Infra-red Spectra and Structure of Organic Compounds), M. Mir, Moscow, Russia, 1965, pp. 23–68.
[31] P. Kubelka, J. Opt. Soc. Am. 38 (5) (1948) 448–457.

[32] S. Sakthivel, H. Kisch, Angew. Chem. Int. Ed. 42 (2003) 4908–4911.
[33] J.K. Vassiliou, V. Mehrotra, M.W. Russell, E.P. Giannelis, J. Appl. Phys. 73 (1993) 5109–5116.
[34] Yu.V. Kolen'ko, B.R. Churagulov, M. Kunst, L. Mazerolles, C. Colbeau-Justin, Appl. Catal. B: Environ. 54 (1) (2004) 51–58.
[35] K. Chhor, J.F. Bocquet, C. Colbeau-Justin, Mater. Chem. Phys. 86 (2004) 123–131.
[36] R.I. Bickley, T. Gonzalez-Carreno, J.S. Lees, L. Palmisano, R.J.D. Tilley, J. Solid State Chem. 92 (1991) 178–190.
[37] B. Sun, A.V. Vorontsov, P.G. Smirniotis, Langmuir 19 (2003) 3151–3156.